

Ferroelastic Behavior of LaCoO₃-Based Ceramics

Kjersti Kleveland, Nina Orlovskaya,* Tor Grande,* Anne Marie Mardal Moe, and Mari-Ann Einarsrud*

Department of Chemistry, Norwegian University of Science and Technology, N-7491 Trondheim, Norway

Kristin Breder*[†]

Oak Ridge National Laboratory, Oak Ridge, Tennessee 3731–6069

George Gogotsi

Institute for Problems of Strength, National Academy of Sciences of Ukraine, Kiev, Ukraine

LaCoO₃ and La_{0.8}Ca_{0.2}CoO₃ ceramics show a nonelastic stress–strain behavior during four-point bending experiments where hysteresis loops are observed during loading–unloading cycles. Permanent strain is stored in the material after unloading, and a mechanism related to ferroelastic domain switching in the rhombohedral perovskite is proposed. Domain switching in the materials has been confirmed using X-ray diffractometry. Fracture toughnesses of La_{0.8}Ca_{0.2}CoO₃ measured using single-edge notched beam and single-edge V-notched beam methods coincide and are equal to 2.2 MPa·m^{1/2} at room temperature and decrease to ~1 MPa·m^{1/2} at temperatures >300°C. A decrease in fracture toughness is consistent with ferroelastic behavior, because the rhombohedral distortion decreases with increasing temperature.

I. Introduction

MONOLITHIC ceramic materials are usually brittle and deform elastically under stress. However, a particular type of ceramics, which shows nonelastic behavior, has been termed ferroelastic by analogy with the stress–strain relationship with the polarization of ferroelectric materials in electrical fields or the magnetization of ferromagnetic materials in magnetic fields.¹ Such nonelastic behavior has been related to domain switching under loading. Ferroelastic behavior has been observed for several ceramic materials, such as tetragonal zirconia (*t*-ZrO₂), zirconates, titanates, and vanadates.^{2–5} Spontaneous ferroelastic strain in rhombohedral perovskites, such as LaAlO₃, has been previously reported by Müller *et al.*⁶ Rhombohedral perovskites should undergo a paraelastic to ferroelastic transition when transforming from cubic to rhombohedral structures during cooling.¹ Pure LaCoO₃ has a rhombohedral structure at room temperature and also has a significant distortion from cubic structure at 1000°C. When the data for the rhombohedral angle are extrapolated, LaCoO₃ remains rhombohedral up to temperatures close to the melting point.^{7–9} At 50 mol% substitution of strontium for lanthanum, the crystal structure becomes cubic.^{10,11} At moderate substitution levels of calcium or strontium ($x = 0.2$), however, the rhombohedral

distortion remains significant at room temperature. The rhombohedral to cubic phase transition is observed at ~900°C for these substituted materials.¹² LaCoO₃-based materials are interesting from an application point of view, because they are potential materials for use as dense ceramic membranes for oxygen separation from air and for synthetic-gas production. Pure LaCoO₃ is a semiconductor at room temperature, whereas substitution with ~20% calcium or strontium for lanthanum gives increased ionic and electronic conductivity, and the materials become metallic.¹⁰

To date, the mechanical properties of lanthanum transition metal oxide perovskites have not received much attention, despite the fact that the high-temperature applications of these types of material demand certain mechanical properties, such as mechanical strength and high creep resistance. Only a few characteristics, such as bending strength and Young's modulus, can be found in the literature for some selected perovskites.^{13–16} The reported data on bending strength are limited to La_{0.9}Sr_{0.1}Ga_{0.8}Mg_{0.2}O_{3–δ}, La_{0.875}Sr_{0.125}MnO_{3+δ}, and La_{0.7}Sr_{0.3}Cr_{1–y}Co_yO₃.^{17–19} In our recent work,²⁰ selected mechanical properties of LaCoO₃, La_{0.8}Sr_{0.2}CoO₃, and La_{0.8}Ca_{0.2}CoO₃ materials containing some amount of secondary phases were investigated. We also observed a nonlinear stress–strain relation for these materials at room temperature. The motivation for the present work, therefore, was to further study the nonlinear stress–strain behavior observed and possibly relate this behavior to ferroelasticity. Furthermore, we wanted to determine the bending strength and fracture toughness of phase-pure LaCoO₃ and La_{0.8}Ca_{0.2}CoO₃.

II. Experimental Procedure

Powders with the stoichiometry LaCoO₃ and La_{0.8}Ca_{0.2}CoO₃ were prepared through a wet chemical route using metal nitrates and ethylenediaminetetraacetic acid (EDTA) as a complexing agent. Stoichiometric amounts of metal nitrates were dissolved in deionized, distilled water and added to EDTA. The complexation took place at 80°C with a pH between 8 and 10. The powders were dried, the organic residue was removed, and the powders were ball milled with Si₃N₄ balls and calcined for 15 h at 950°C for LaCoO₃ and 900°C for La_{0.8}Ca_{0.2}CoO₃. The cooling rate was 200 K/h. The powders were further ball milled and pressed into bars (6 mm × 10 mm × 55 mm) at a uniaxial pressure of 30 MPa, followed by cold isostatic pressing at 300 MPa. LaCoO₃ powders were sintered at 1200°C for 24 h, and La_{0.8}Ca_{0.2}CoO₃ powders were sintered at the same temperature for 10 or 65 h. The cooling rate was 25 K/h to 600°C, followed by 100 K/h to room temperature.

The samples were characterized using powder X-ray diffraction (XRD; Model D5005 diffractometer with CuK α -radiation and secondary monochromator, Siemens, Karlsruhe, Germany) and scanning electron microscopy (SEM; Model DSM 940, Zeiss,

K. T. Faber—contributing editor

Manuscript No. 188075. Received December 19, 2000; approved May 29, 2001. Supported by the Research Council of Norway.

*Member, American Ceramic Society.

[†]Present address: Higgins Grinding Technology Center, Saint-Gobain Abrasives, Worcester, MA.

Oberkochen, Germany). Three types of ceramic surfaces were investigated: polished surface (0.25 μm diamond), machined surface (Military Standard 1942B), and the machined surface after annealing at 1100°C for 4 h. No secondary phases were observed in the powders or sintered samples. The bulk density of the ceramics was determined using the Archimedes method with isopropyl alcohol. Some characteristics of the samples are given in Table I. The grain size of LaCoO_3 was somewhat larger than that of $\text{La}_{0.8}\text{Ca}_{0.2}\text{CoO}_3$, and the porosity of LaCoO_3 was significantly higher than that of the calcium-substituted samples.

Stress–strain relationships and four-point bending strength (“Standard Test Method for Flexural Strength of Advanced Ceramics at Ambient Temperature,” ASTM Designation C1161. American Society for Testing and Materials, West Conshohocken, PA) were measured for both compositions at room temperature. Testing at room temperature was performed in a four-point flexure with 40 and 20 mm spans (Model 1126 and Model 880 control panel, Instron Corp., Danvers, MA). The load cell was 5 kN. Displacement was measured using a Tesa-type displacement gauge (± 0.5 mm, maximum error of 0.2 μm) placed in contact with the sample in the center of the span. The displacement gauge was fixed such that it measured the displacement relative to the load points. Loading point and supports were free to roll; their diameters were 4.9 mm. Cycling was performed by consequently loading and unloading the sample either up to the same maximum load or by increasing the maximum load for each cycle. The cycling was performed automatically, using the control panel to avoid holding times at either zero or maximum load. All measurements were performed in displacement control, with displacement of crosshead controlled from the machine (no feedback from the displacement gauge). The crosshead rate was normally 0.5 mm/min; however, measurements were performed in the range 0.5–0.005 mm/min. All samples were nominally 3 mm \times 4 mm \times 45 mm. About 10 samples of each composition were taken to fracture to record bending strength at room temperature.

Fracture toughness was determined using the single-edge V-notched beam (SEVNB) method.^{21–23} Rectangular bars (nominally 3 mm \times 4 mm \times 45 mm) were prenotched using a diamond blade followed by forming the V-notch by filling the preliminary notch with a diamond paste (2–7 μm grain size) and using a razor blade (100–300 μm in thickness). The notch length and radius were measured using optical microscopy and SEM. The fracture toughness measurements were performed using a four-point bending fixture (20 and 40 mm geometry) previously described by Gogotsi.²¹ The crosshead speed was 0.5 mm/min. Normally, two samples were recorded for each of the temperatures 200°, 300°, 600°, and 800°C.

III. Results and Discussion

(I) Nonelastic Behavior

The porous LaCoO_3 and the dense $\text{La}_{0.8}\text{Ca}_{0.2}\text{CoO}_3$ ceramics show a nonelastic stress–strain behavior during the four-point bending experiments, as shown in Fig. 1. Loading–unloading cycling to consequently higher loads during four-point bending of $\text{La}_{0.8}\text{Ca}_{0.2}\text{CoO}_3$ reveals reproducible hysteresis loops, as shown in Fig. 2(a). The stress–strain hysteresis behavior does not depend on the loading rate within the range 0.5–0.005 mm/min; however, the width of the loop increases with increasing maximum load, as

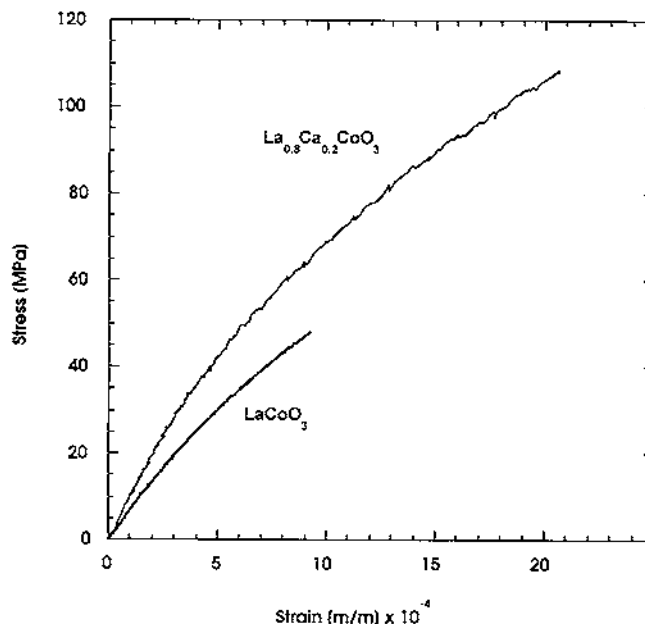


Fig. 1. Stress–strain relationship during four-point bending of LaCoO_3 and $\text{La}_{0.8}\text{Ca}_{0.2}\text{CoO}_3$ at room temperature.

shown in Fig. 2(a). Figure 2(a) shows that some residual strain is stored in the material after loading. Compared with the finite-element calculations performed by Steinkopff,²⁴ the present results point to a ferroelastic behavior caused by domain switching of this perovskite. The rigidity of the setup has been checked using a dense sintered SiC sample, and this sample shows completely elastic behavior during loading–unloading.

The characteristic for a ferroelastic material is an elastic hysteresis in the stress–strain relation, and a permanent strain is present in the materials after unloading.^{1,25} Figure 2(a) shows only a part of an elastic hysteresis loop for a ferroelastic material. To study the complete hysteresis loop caused by ferroelasticity, the material has to be subjected to pure compressive stresses, followed by tensile stresses (or a shear stress that allows easy reversion of the direction of loading). For the present investigation, a four-point bending setup was used; hence, the sample bar was in tension and under compression on either side of the bar. The part of the hysteresis curves in Fig. 2(a) obtained during loading constitutes a part of the total hysteresis loop for this material. However, because of the low flexure strength of these samples caused by large voids/pores, we have measured only the low-stress part of the expected total hysteresis loop before fracture. A saturation point is expected at higher stresses. This, however, is observed during loading–unloading at 600°C. At this temperature, a smaller deviation from cubic structure is reported,¹² and, hence, the energy of domain switching is lower, and the hysteresis loops are narrower.

The loading–unloading behavior was further studied by turning the sample bar upside down in the sample holder after one stress–strain cycle (Fig. 2(b)). The surface previously under compression was now in tension and vice-versa for the first loading–unloading cycle. Figure 2(b) shows that the strains generated on the compression side in the first cycle have to be overcome in the first cycle after the turning and that a permanent strain is observed after the end of the first cycle. The residual strain is lower than what has been measured during four-point bending of lead zirconate titanate- (PZT-) based ceramics.²⁶ Consecutive cycles measured on the same side follow the same course as before turning the sample bar. The slope of the stress–strain curve representing Young’s modulus is smaller for the first cycle after turning compared with the following cycles, and the calculated Young’s moduli for the first and second loops are 105 and 115 GPa, respectively, using the stress–strain data for the low-stress loads. It might be argued that the nonlinear stress–strain behavior

Table I. Sintering Time, Grain Size, Density, and Porosity of Samples Used for Mechanical Testing

Sample	Sintering time at 1200°C (h)	Grain size (μm)	Density (g/cm^3)	Porosity (%)
LaCoO_3	24	4–6	6.75	7.4
$\text{La}_{0.8}\text{Ca}_{0.2}\text{CoO}_3$	65 [†]	3–5	6.62	1.6
$\text{La}_{0.8}\text{Ca}_{0.2}\text{CoO}_3$	10	1–2	6.59	2.0

[†]Used for high-temperature measurements, SEVNB method, and for XRD measurements.

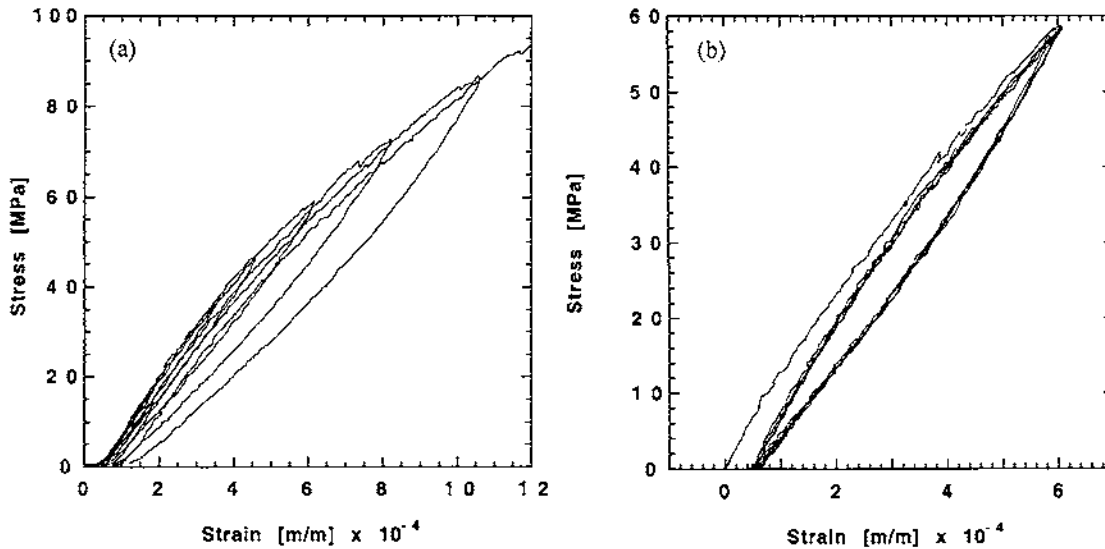


Fig. 2. Cyclic four-point bending test below the fracture stress of $\text{La}_{0.8}\text{Ca}_{0.2}\text{CoO}_3$ at room temperature. (a) Six cycles up to consecutively higher loads; sample not taken to fracture. (b) Bar turned upside down after a previous test; hence, the tensile surface was in compression and vice versa during the first cycle (four cycles are shown).

observed in Fig. 1 is due to microcracking in the sample, but a higher slope of the stress-strain curve for the second cycle is not consistent with such a mechanism. Therefore, we conclude that the permanent strain observed is due to ferroelasticity. Fett *et al.*²⁷ have previously observed that there is a nonlinear and nonsymmetric stress distribution around the neutral axis in PZT ceramics during beam bending and that the tensile strains are larger than the compressive strains for the same stress level. Such behavior also has been modeled for ferroelastic materials using the finite-element method.²⁴ The data in Fig. 2(b) also infer that the stress-strain relationship is different under compression and in tension. A possible explanation for the permanent strain observed is that domain reorientation in a certain direction is facilitated under compression compared with tension. However, our observations call for further investigations to completely understand the behavior.

XRD of the ceramic surfaces having various mechanical and thermal histories has been conducted to gain additional evidence of ferroelastic behavior and domain switching. The (110) and (104) reflections of LaCoO_3 and $\text{La}_{0.8}\text{Ca}_{0.2}\text{CoO}_3$ from calcined powders, polished surface, machined surface, and machined surface after annealing at 1100°C for 4 h are shown in Fig. 3. The intensity ratio I_{110}/I_{104} and full-width at half-maximum (FWHM) for all the diffractograms are summarized in Table II. The lattice parameters and the intensities observed for LaCoO_3 powders are in good agreement with literature data.^{10,11} The X-ray patterns of the powders correspond to a random orientation of domains and, thereby, reflect the true structure factors of the two peaks for both compositions. The intensity ratio I_{110}/I_{104} for the polished surfaces of the materials is almost equal to the corresponding value obtained for the powders; only small texture due to preferred orientation of domains appears on the polished surfaces. The intensity ratio I_{110}/I_{104} of the machined surfaces, however, is significantly higher than that of the powders and polished surfaces (Table II). The diffraction patterns clearly demonstrate that the (104) reflection decreases substantially after the mechanical treatment. The implication is that the stresses induced during machining must be in excess of the coercive stress necessary for the reorientation of the ferroelastic domains. The majority of the domains, therefore, have reoriented in such a way that their (001) axes are almost parallel to the surface. As a result, the intensity of the (104) reflection decreases while the (110) intensity remains unchanged within the uncertainty of the measurement. Similar effects also have been observed for other reflections, resulting in weakening of reflections with nonzero l indexes. Significant

broadening of peaks is observed for the surfaces after machining compared with polishing. The broadening is probably partly due to residual stresses and strains introduced by machining. More careful studies are necessary to understand the nature of the broadening of the XRD reflections.

The diffraction patterns of the machined surfaces after annealing at 1100°C are also shown in Fig. 3. The intensity ratio I_{110}/I_{104} of $\text{La}_{0.8}\text{Ca}_{0.2}\text{CoO}_3$ after the thermal treatment results in a transformation back to almost random orientation of the domains. Therefore, we conclude that the ferroelastic to paraelastic transition of $\text{La}_{0.8}\text{Ca}_{0.2}\text{CoO}_3$ occurs below 1100°C , which is consistent with the reported change from rhombohedral to cubic structure at $\sim 900^\circ\text{C}$.¹² The intensity ratio I_{110}/I_{104} of LaCoO_3 does not change significantly because of the thermal treatment at 1100°C , as shown in Fig. 3(a). From crystallographic data,^{8,9} the rhombohedral to cubic transition of pure LaCoO_3 is expected to occur far above 1100°C , which corresponds well with the present observation.

The microstructure of LaCoO_3 -based materials has been recently investigated using transmission electron microscopy (TEM) by Walmsley *et al.*²⁸ They have found that the most prominent microstructural feature of $\text{La}_{0.8}\text{Ca}_{0.2}\text{CoO}_3$ material is the presence of twinning on {012} pseudo-cubic planes. On either side of the twin boundaries, the crystal has rhombohedral $\langle 001 \rangle$ axes lying in different directions. The three variants have rhombohedral axes lying parallel to the $\langle 111 \rangle$ directions of the high-temperature cubic cell. The twin lamellas reflect the increasing rhombohedral distortion from cubic symmetry during cooling after densification. Similar twin domains have been observed in other ferroelastic materials.¹

(2) Bending Strength and Fracture Toughness

Four-point bending strength of $\text{La}_{0.8}\text{Ca}_{0.2}\text{CoO}_3$ has been measured to be 111 ± 18 MPa at room temperature. The strength of these types of materials previously has been shown to decrease with increasing temperature.²⁰ The room-temperature strength of LaCoO_3 is ~ 65 MPa. The fracture origin is large voids or pores for all the samples; however, the size of the voids is larger and the porosity is higher for LaCoO_3 than for $\text{La}_{0.8}\text{Ca}_{0.2}\text{CoO}_3$. The theoretical strength of LaCoO_3 and $\text{La}_{0.8}\text{Ca}_{0.2}\text{CoO}_3$ is expected to be relatively equal; however, $\text{La}_{0.8}\text{Ca}_{0.2}\text{CoO}_3$ to some extent is stronger because of the higher valence of cobalt. The low strength of LaCoO_3 , therefore, reflects the higher level of porosity and larger fracture origin size. The fracture mode is mostly transgranular for both compositions at room temperature, whereas mostly an

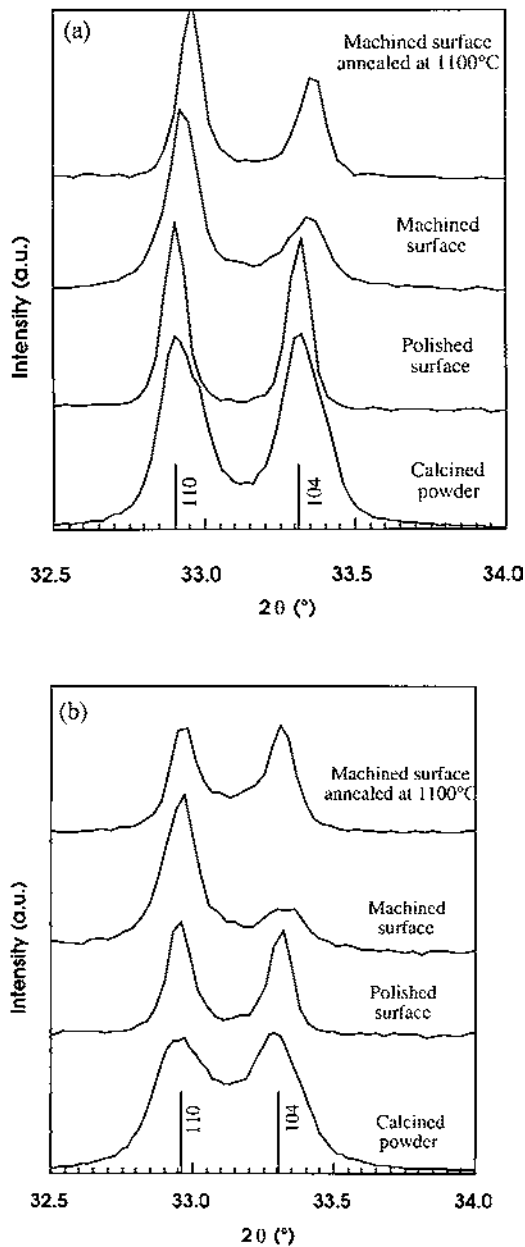


Fig. 3. XRD trace of (a) LaCoO_3 and (b) $\text{La}_{0.8}\text{Ca}_{0.2}\text{CoO}_3$ polycrystalline ceramics and powders. Two reflections shown correspond to the (left) (110) and (right) (104) reflections, respectively.

intergranular mode is obtained for the $\text{La}_{0.8}\text{Ca}_{0.2}\text{CoO}_3$ samples tested at elevated temperatures. The change in fracture mode with temperature indicates a weakening of the grain boundaries at elevated temperatures.

Fracture toughness of $\text{La}_{0.8}\text{Ca}_{0.2}\text{CoO}_3$ measured using the SEVNB method as a function of temperature is shown in Fig. 4.

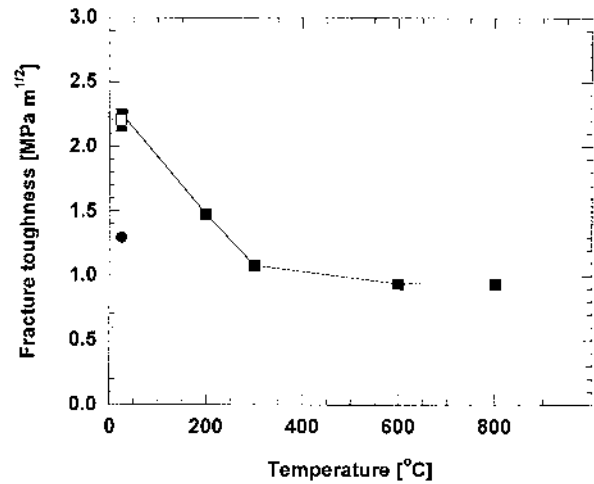


Fig. 4. Fracture toughness of (■) $\text{La}_{0.8}\text{Ca}_{0.2}\text{CoO}_3$ measured using SEVNB as a function of temperature. Fracture toughnesses of (●) LaCoO_3 (SEVNB) and (□) $\text{La}_{0.8}\text{Ca}_{0.2}\text{CoO}_3$ (SENB) measured at room temperature are shown.

For comparison, the fracture toughness of LaCoO_3 (SEVNB) and $\text{La}_{0.8}\text{Ca}_{0.2}\text{CoO}_3$ (SENB) measured at room temperature is included in Fig. 4. The fracture toughness of $\text{La}_{0.8}\text{Ca}_{0.2}\text{CoO}_3$ ($2.2 \text{ MPa}\cdot\text{m}^{1/2}$) is almost 2 times higher than the fracture toughness of pure LaCoO_3 ($1.3 \text{ MPa}\cdot\text{m}^{1/2}$) at room temperature. This coincides with the bending strength ratio. Because of the relatively high fracture toughness of $\text{La}_{0.8}\text{Ca}_{0.2}\text{CoO}_3$ at room temperature, we propose that toughening caused by domain reorientation occurs, as also has been reported for t' - ZrO_2 .²⁹ The decrease in fracture toughness with increasing temperature is consistent with a decrease in rhombohedral angle for this material; however, the fracture toughness shows a faster decrease with temperature than does the rhombohedral angle. The fast decrease might be due to increased thermal energy and, hence, a lower energy for domain reorientation. The fracture toughness of pure LaCoO_3 at room temperature is significantly less than for $\text{La}_{0.8}\text{Ca}_{0.2}\text{CoO}_3$. Further work is in progress to understand that LaCoO_3 shows a lower fracture toughness. However, at present, the following factors are relevant: higher porosity, higher energy for domain reorientation (higher deviation from cubic symmetry), lower number of domains able to reorient, and paraelastic to ferroelastic phase transition temperature is higher than the sintering temperature.⁸

IV. Conclusions

LaCoO_3 and $\text{La}_{0.8}\text{Ca}_{0.2}\text{CoO}_3$ perovskites show a nonelastic stress-strain behavior during four-point bending experiments, and hysteresis loops are formed during cycling. Residual strain is stored in the material after loading, and a mechanism related to ferroelastic domain switching in the rhombohedral perovskite is proposed. XRD shows that the intensity ratio between the (110)

Table II. Ratio of the Intensity of the (110) and (104) Reflections and Full-Width at Half-Maximum of the (110) and (104) Reflections of LaCoO_3 and $\text{La}_{0.8}\text{Ca}_{0.2}\text{CoO}_3$ Measured Using XRD

Sample	LaCoO_3			$\text{La}_{0.8}\text{Ca}_{0.2}\text{CoO}_3$		
	$I_{(110)}/I_{(104)}$	FWHM		$I_{(110)}/I_{(104)}$	FWHM	
		(110)	(104)		(110)	(104)
Calcined powder	1.01	0.1288	0.1315	1.03	0.2242	0.2154
Polished surface	1.12	0.0843	0.0869	1.21	0.1048	0.0954
Machined surface	1.88	0.1135	0.1691	4.39	0.1389	0.1961
Machined surface after annealing at 1100°C	1.83	0.0923	0.1150	0.93	0.1222	0.1333

and (104) reflections changes when the ceramic surface is machined. The implication is that the stresses induced during machining must be in excess of the coercive stress necessary for the reorientation of ferroelastic domains. The intensity ratio I_{110}/I_{104} of La_{0.8}Ca_{0.2}CoO₃ after the thermal treatment at 1100°C results in a transformation back to almost random orientation of the domains because of crossing the ferroelastic to paraelastic transition. The bending strength for 98%-dense La_{0.8}Ca_{0.2}CoO₃ is 111 ± 18 MPa at room temperature. Large pores/defects are decisive for the strength. Fracture toughnesses of La_{0.8}Ca_{0.2}CoO₃ measured by the SENB and SEVNB methods at room temperature coincide and are equal to 2.2 MPa·m^{1/2}. The fracture toughness measured by the SEVNB method decreases to ~1 MPa·m^{1/2} at temperatures >300°C. The decrease in fracture toughness is consistent with the proposed ferroelastic domain reorientation mechanism, where we have ferroelastic toughening at room temperature.

References

- ¹E. K. H. Salje, *Phase Transition in Ferroelastic and Co-elastic Crystals*. Cambridge University Press, Cambridge, U.K., 1990.
- ²A. V. Virkar and R. L. K. Matsumoto, "Ferroelastic Domain Switching as a Toughening Mechanism in Tetragonal Zirconia," *J. Am. Ceram. Soc.*, **69** [10] C-224–C-226 (1986).
- ³K. Mehta and A. V. Virkar, "Fracture Mechanism in Ferroelectric–Ferroelastic Lead Zirconate Titanate (Zr:Ti = 0.54:0.46) Ceramics," *J. Am. Ceram. Soc.*, **73** [3] 567–74 (1990).
- ⁴F. Meschke, A. Kolleck, and G. A. Schneider, "R-Curve Behavior of BaTiO₃ due to Stress-Induced Ferroelastic Domain Switching," *J. Eur. Ceram. Soc.*, **17**, 1143–49 (1997).
- ⁵T. L. Baker, K. T. Faber, and D. W. Ready, "Ferroelastic Toughening in Bismuth Vanadate," *J. Am. Ceram. Soc.*, **74**, 1619–23 (1991).
- ⁶K. A. Müller, W. Berlinger, and F. Waldner, "Characteristic Structural Phase Transition in Perovskite-Type Compounds," *Phys. Rev. Lett.*, **21** [12] 814–17 (1968).
- ⁷J.-P. Coutures, J. M. Badie, R. Berjoan, J. Coutures, R. Flamand, and A. Rouanet, "Stability and Thermodynamic Properties of Rare-Earth Perovskites," *High Temp. Sci.*, **13**, 331–36 (1980).
- ⁸B. Gilbu, H. Fjellvåg, and A. Kjekshus, "Properties of LaCo_{1-x}Cr_xCoO₃: Solid Solubility, Thermal Expansion, and Structural Transition," *Acta Chem. Scand.*, **48**, 37–45 (1994).
- ⁹G. Thornton, B. C. Tofield, and A. W. Hewat, "A Neutron Diffraction Study of LaCoO₃ in the Temperature Range $4 < T < 1248$ K," *J. Solid State Chem.*, **61**, 301–307 (1986).
- ¹⁰A. Mineshige, M. Inaba, T. Yao, Z. Ogumi, K. Kikuchi, and M. Kawase, "Crystal Structure and Metal–Insulator Transition of La_{1-x}Sr_xCoO₃," *J. Solid State Chem.*, **121**, 423–29 (1996).
- ¹¹R. Caciuffo, D. Rinaldi, G. Barucca, J. Mira, J. Rivas, M. A. Snaris-Rodriguez, P. G. Radaelli, D. Fiorani, and J. B. Goodenough, "Structural Details and Magnetic Order of La_{1-x}Sr_xCoO₃ ($x \leq 0.3$)," *Phys. Rev. B: Condens. Matter*, **59** [2] 1068–78 (1999).
- ¹²S. Faaland, M. Menom, M.-A. Binarsrud, and T. Grande, "Phase Transition and Thermal Expansion of Calcium-Strontium-Substituted Lanthanum Cobaltite," *J. Mater. Chem.*, in review.
- ¹³A. Selcuk and A. Atkinson, "Elastic Properties of Ceramic Oxides Used in Solid Oxide Fuel Cells (SOFC)," *J. Eur. Ceram. Soc.*, **17**, 1523–32 (1997).
- ¹⁴C. S. Montross, H. Yokokawa, M. Doliya, and L. Bekessy, "Mechanical Properties of Magnesia-Doped Lanthanum Chromite versus Temperature," *J. Am. Ceram. Soc.*, **78**, 1869–72 (1995).
- ¹⁵M. Mori, H. Itoh, N. Mori, and T. Abe, "Mechanical and Electrical Properties of Alkaline-Earth-Doped Lanthanum Chromites"; pp. 325–34 in *Proceedings of the 3rd International Symposium on Solid Oxide Fuel Cells*. Edited by S. C. Singhal and H. Iwahara. Electrochemical Society, Tokyo, Japan, 1997.
- ¹⁶K. Li, X. Li, Ch. Lui, Zh. Zhu, J. Du, D. Hou, X. Nie, J. Zhu, and Y. Zhang, "Magnetically Correlated Internal Friction and Young's Modulus in La(Y)-Ca-Mn-O Perovskites," *Phys. Rev. B: Condens. Matter*, **56**, 13662–65 (1997).
- ¹⁷J. Drennan, V. Zelizko, D. Hay, F. T. Ciacchi, S. Rajendran, and S. P. S. Badwal, "Characterization, Conductivity, and Mechanical Properties of Oxygen-Ion Conductor La_{0.9}Sr_{0.1}Ga_{0.8}Mg_{0.2}O_{3-x}," *J. Mater. Chem.*, **7** [1] 79–83 (1997).
- ¹⁸C. M. D'Souza and N. M. Sammes, "Mechanical Properties of Strontium-Doped Lanthanum Manganite," *J. Am. Ceram. Soc.*, **83**, 47–52 (2000).
- ¹⁹N. M. Sammes and R. Ratnaraj, "High-Temperature Mechanical Properties of La_{0.7}Sr_{0.3}Cr_{1-x}Co_xO₃ in Reducing Environments," *J. Mater. Sci.*, **32**, 687–92 (1997).
- ²⁰N. Orlovskaya, K. Kleveland, T. Grande, and M. A. Einarsrud, "Mechanical Properties of LaCoO₃-Based Ceramics," *J. Eur. Ceram. Soc.*, **20**, 51–56 (2000).
- ²¹G. A. Gogotsi, "Crack Resistance of Ceramics and Composites with Ceramic Matrix (SEVNB Method)," *Tekh. Keram.*, **11**, 7–13 (1999).
- ²²H. Awaji and Y. Sakaida, "V-Notch Technique for Single-Edge Notched Beam and Chevron Notch Methods," *J. Am. Ceram. Soc.*, **73** [11] 3522–23 (1990).
- ²³J. Kübler, "Fracture Toughness Using SEVNB Method: Preliminary Results," *Ceram. Eng. Sci. Proc.*, **18** [4] 155–62 (1997).
- ²⁴Th. Steinkopf, "Micromechanical Modeling of Ferroelasticity and Ferroelectricity and Finite-Element Results for Nonlinear Piezoelectric Applications," *Ferroelectrics*, **222**, 125–29 (1999).
- ²⁵V. K. Wadhawan, "Ferroelasticity: Introductory Survey and Present Status," *Phase Transitions*, **34**, 3–18 (1991).
- ²⁶R. A. Pferner, G. Thurn, and F. Aldinger, "Mechanical Properties of PZT Ceramics with Tailored Microstructure," *Mater. Chem. Phys.*, **61**, 24–30 (1999).
- ²⁷T. Fett, D. Munz, and G. Thurn, "Nonsymmetric Deformation Behavior of Lead Zirconate Titanate Determined in Bending Tests," *J. Am. Ceram. Soc.*, **81** [1] 269–72 (1998).
- ²⁸J. C. Walmsley, A. Bardal, K. Kleveland, M.-A. Einarsrud, and T. Grande, "Microstructure and the Influence of Spontaneous Strain in LaCoO₃, La_{0.8}Sr_{0.2}CoO₃, and La_{0.8}Ca_{0.2}CoO₃," *J. Mater. Sci.*, **35**, 4251–60 (2000).
- ²⁹A. Foitzik, M. Stadtwald-Klenke, and M. Rühle, "Ferroelasticity of t'-ZrO₂," *Z. Metallkd.*, **84**, 397–404 (1993). □